^{15}N NMR Relaxation Studies of Backbone Dynamics in Free and Steroid-Bound Δ^5-3-Ketosteroid Isomerase from *Pseudomonas testosteroni*†

Sunggoo Yun,‡,§ Do Soo Jang,|| Do-Hyung Kim,§,|| Kwan Yong Choi,§,|| and Hee Cheon Lee*,‡,§

Department of Chemistry, Center for Biofunctional Molecules, and Division of Molecular and Life Sciences, Pohang University of Science and Technology, Pohang, 790-784 Korea

Received October 3, 2000; Revised Manuscript Received January 9, 2001

ABSTRACT: The backbone dynamics of Δ^5-3-ketosteroid isomerase (KSI) from *Pseudomonas testosteroni* has been studied in free enzyme and its complex with a steroid ligand, 19-nortestosterone hemisuccinate (19-NTHS), by ^{15}N relaxation measurements. The relaxation data were analyzed using the model-free formalism to extract the model-free parameters (S^2, τ_e, and R_{ex}) and the overall rotational correlation time (τ_m). The rotational correlation times were 19.23 ± 0.08 and 17.08 ± 0.07 ns with the diffusion anisotropies ($D_\parallel/D_\perp$) of 1.26 ± 0.03 and 1.25 ± 0.03 for the free and steroid-bound KSI, respectively. The binding of 19-NTHS to free KSI causes a slight increase in the order parameters (S^2) for a number of residues, which are located mainly in helix A1 and strand B4. However, the majority of the residues exhibit reduced order parameters upon ligand binding. In particular, strands B3, B5, and B6, which have most of the residues involved in the dimer interaction, have the reduced order parameters in the steroid-bound KSI, indicating the increased high-frequency (pico- to nanosecond) motions in the intersubunit region of this homodimeric enzyme. Our results differ from those of previous studies on the backbone dynamics of monomeric proteins, in which high-frequency internal motions are typically restricted upon ligand binding.

Protein dynamics both in catalysis and in specific ligand binding is a subject of great interest, because it can markedly influence the important aspects of protein functions, such as folding (*1*, *2*), molecular recognition, stability, and enzyme action (*3*). Especially, the specific intermolecular interactions between a ligand and the protein can alter the internal motions in a wide range of time scales. Heteronuclear NMR[1] has been widely used to study such internal motions of proteins, because ^{13}C and ^{15}N NMR relaxation measurements provide unique experimental data for the side chain and backbone dynamics in a wide range of time scales from pico- to milliseconds. For instance, the model-free analysis (*4*, *5*) of the relaxation data provides dynamical information of the internal motions on the pico- and nanosecond time scale parametrized as the spatial restriction of the N−H (or C−H) vector orientation (S^2, generalized order parameter), the effective correlation time of the internal motion (τ_e, pico- to nanosecond time scale), rotational tumbling of the whole molecule (τ_m, nanosecond time scale), and the microenvironment change on the micro- to millisecond time scale (R_{ex}).

The dynamics of the backbone and side chain in several free and ligand-bound proteins have been investigated using ^{2}H (*6*, *7*), ^{13}C (*8*, *9*), and ^{15}N (*10*−*16*) NMR relaxation experiments. The results of many of these studies showed that ligand binding induces a localized restriction of the side chain and backbone motion near the ligand binding site. However, some of them (*10*, *14*, *16*) suggested that a number of distal residues become more mobile in complex formation, while the binding site residues become more rigid. Such increased mobility of the distal residues upon ligand binding was interpreted as a mechanism for reducing the unfavorable entropy associated with binding site rigidification.

Ketosteroid isomerase (KSI) is a homodimeric enzyme with 125 amino acid residues per subunit which catalyzes the conversion of Δ^5- to Δ^4-3-ketosteroid via a dienolic intermediate with diffusion-controlled rate. This enzyme has a molecular mass of 26.8 kDa and consists of three α-helices and a six-strand mixed β-pleated sheet that contains three β-bulges. Three-dimensional structures in solution as well as those in the crystal state have been identified by NMR and X-ray crystallography (*17*, *18*). Figure 1 shows that the structure of KSI is a conical closed barrel formed by a highly curved β-sheet and three α-helices. The α-helices are adjacent to each other and arranged in an antiparallel orientation. The narrow end of the structure is blocked, while the wide end is open to the bulk solvent forming an active site. A narrow and long patch of the β-sheet of each monomer forms a dimer interface, where the interactions are mostly between side chains and are hydrophobic in nature.

† This work was supported by a grant from POSCO R & D (1999) and by the Korea Science Engineering Foundation.

* To whom correspondence should be addressed. Tel: 82-054-279-2116. Fax: 82-054-279-3399. E-mail: hcl@postech.ac.kr.

‡ Department of Chemistry.

§ Center for Biofunctional Molecules.

|| Division of Molecular and Life Sciences.

[1] Abbreviations: KSI, ketosteroid isomerase; 19-NTHS, 19-nortestosterone hemisuccinate; DMSO, dimethyl sulfoxide; NMR, nuclear magnetic resonance; HSQC, heteronuclear single-quantum coherence; T_1, longitudinal relaxation time; T_2, transverse relaxation time; NOE, nuclear Overhauser effect; S^2, generalized order parameter; τ_e, effective correlation time for internal motions; τ_m, overall rotational correlatin time; R_{ex}, conformational exchange term; WALTZ, *w*ide-band *a*lternating-phase *l*ow-power *t*echnique for *z*ero residual splitting; CPMG, Carr−Purcell−Meiboom−Gill multipulse sequence; WATERGATE, water suppression by gradient-tailored excitation.

10.1021/bi0023192 CCC: $20.00
Published on Web 03/06/2001

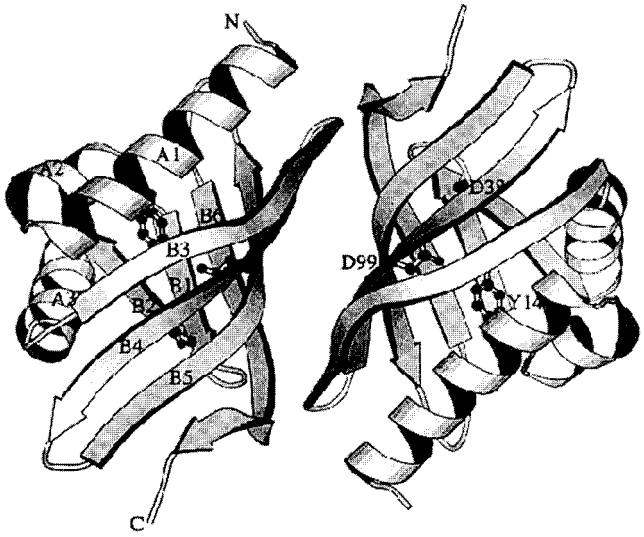

FIGURE 1: Dimeric structure of KSI viewed roughly along the molecular 2-fold axis. A and B correspond to α-helix and *β*-strand, respectively. The three major catalytic residues are shown in ball-and-stick models.

Zhao et al. (*9*) examined the side chain and backbone dynamics of the catalytic residue, Tyr-14, in a mutant KSI, Y55F/Y88F, by ^{13}C NMR relaxation measurement in the presence and absence of a steroid ligand, 19-nortestosterone hemisuccinate (19-NTHS). The results showed that the high-frequency (pico- to nanosecond) motion of the phenolic side chain C_ϵ became more restricted than that of the backbone C_α upon binding of 19-NTHS, while the ligand binding decreased the low-frequency (micro- to millisecond) motion of C_α but produced no change in that of C_ϵ. On the other hand, the solution structures of free and 19-NTHS-bound KSI indicate that three α-helices change their position upon ligand binding, becoming more closely packed onto the concave surface of the *β*-sheet in the complexed KSI, thus bringing Tyr-14 closer to Asp-99 and the substrate (*19*). Therefore, it seems that ligand binding may induce changes in dynamics of more residues in other regions of KSI including the catalytic residues, which could affect the mechanistic action of KSI.

To further elucidate the dynamical changes in KSI upon ligand binding, we have investigated the complete backbone dynamics of free KSI and its complex with 19-NTHS by ^1H-detected ^{15}N NMR relaxation measurements. Motional parameters (S^2, τ_e, and R_{ex}) were extracted from the relaxation data using the model-free formalism (*4*, *5*), and differences in the dynamics of free and complexed KSI were discussed on the basis of structural features of the enzyme.

EXPERIMENTAL PROCEDURES

Materials. 19-Nortestosterone hemisuccinate obtained from Steraloids (Wilton, NH) showed a single spot on thin-layer chromatography and was used without further purification. Buffer salts and DMSO-d_6 were from Sigma (St. Louis, MO). ^{15}N-Labeled NH_4Cl was purchased from Cambridge Isotope Laboratories, Inc. (Andover, MA).

Expression and Purification of Labeled KSI. A single colony of *Escherichia coli* BL21 (DE3) (pLysS) (Novagen, Madison, WI) harboring pKSI-TI (*18*) was used to inoculate 5 mL of M9 minimal medium and grown at 37 °C for 15−20 h. One and one-half milliliter of the culture was transferred to 50 mL of the minimal medium, and then cells were grown further at 37 °C for 10 h. Bacterial cells were diluted 50-fold into M9 medium supplemented with 0.1% (w/v) of ^{15}N-labeled NH_4Cl (99% ^{15}N) and 2×10^{-4}% (w/v) of thiamin and biotin and then grown at 37 °C until the absorbance at 600 nm reached 0.7. After addition of isopropyl α-thiogalactopyranoside to the final concentration of 0.6 mM, the cells were further incubated for 5 h. The labeled protein was collected by centrifugation and purified to homogeneity by deoxycholate affinity chromatography and Superose 12 gel filtration chromatography according to the procedures reported previously (*20*). The homogeneity of the protein was confirmed by the presence of a single band on SDS−polyacrylamide gels stained with Coomassie blue.

Preparation of the NMR Sample. NMR samples were prepared to contain 1.0 mM uniformly ^{15}N-labeled- protein in 10 mM potassium phosphate, 9% (v/v) DMSO-d_6, and 91% H_2O. The pH of the sample was adjusted to 7.0. To obtain the protein complexed with a steroid, 19-NTHS was added to the protein solution with a slightly excess amount of inhibitor relative to that of the protein. The binding dissociation constant, K_d, of 19-NTHS inhibitor is 5.5 ± 1.0 *μ*M (*21*).

NMR Measurements and Processing. All NMR data were collected at 27 °C on a Bruker DRX500 spectrometer (500.13 MHz for ^1H and 50.7 MHz for ^{15}N) equipped with a triple resonance, pulse field gradient probe with actively shielded *z*-axis gradients and a gradient amplifier unit. The pulse sequences used to record ^{15}N T_1, T_2, and steady-state ^{15}N-$\{^1H\}$ NOE spectra were those described by Barbato et al. (*22*) with a slight modification to include water flip-back (*23*) and WATERGATE (*24*) techniques for eliminating the water resonance. Decoupling of ^{15}N spins during acquisition was performed using a WALTZ-16 composite pulse sequence with a field strength of 2 kHz. The observed ^1H chemical shifts were determined relative to the internal reference, sodium 2,2-dimethyl-2-silapentane-5-sulfonate (DSS), which was reported to be insensitive to changes in temperature. Indirect referencing was used for ^{15}N chemical shifts using the frequency ratio of $\omega_N/\omega_H = 0.101\ 329\ 118$ for DSS in water (*25*).

The T_1 and T_2 measurements were performed using a total of 60 transients per t_1 experiment. A total of 128×2048 complex points were acquired in the $t_1 \times t_2$ dimensions. A total of 9 data sets were collected to measure T_1 with delay values: 5, 150, 300, 500, 700, 900, 1100, 1400, and 1700 ms. A total of 10 data sets were collected to measure T_2 with delay values: 0, 5.6, 11.2, 28, 33.6, 44.8, 56, 67.2, 78.4, and 95.2 ms. T_2 measurements utilized a 100 *μ*s delay between sequential ^{15}N pulses in the CPMG pulse train for attenuating the ^{15}N signal loss during a T_2 relaxation period. The field strength of the refocusing pulses in the CPMG pulse sequence was 3.3 kHz. To suppress effects of cross-correlation between $^1H-^{15}N$ dipolar and ^{15}N CSA relaxation mechanisms in the T_1 and T_2 experiments, WALTZ-16 and ^1H 180° pulses were applied during the recovering delays as described (*26*−*28*). A 4 s relaxation delay was used between scans. Heteronuclear steady-state $^{15}N\{^1H\}$ NOE were determined from spectra recorded with (NOE) and without (control) saturation of protons, where saturation was achieved by a train of 120° pulses separated by 5 ms for 5

s. The NOE measurements were performed using a total of 96 transients per t_1 experiment. The t_1 dimension was zero-filled to 256 real data points, and a 90° phase-shifted sine -bell window function was applied prior to Fourier transformation and baseline correction in both dimensions.

Analysis of the Relaxation Parameters. ^{15}N relaxation parameters were analyzed with the model-free method (*4*, *5*) by using the program Modelfree v. 4.0 (*29*, *30*). The cross-peak intensities were measured as peak volumes in order to increase sensitivity (*31*), and the relaxation parameters of too much overlapped peaks were not measured. The difference between parallel and perpendicular components of the ^{15}N chemical shift tensor ($\sigma_{\parallel} - \sigma_{\perp}$) was taken to be −170 ppm (*32*, *33*). T_1 and T_2 were obtained by nonlinear fitting of single exponential decays to the experimental data. The error levels in T_1 and T_2 were estimated by a 500 Monte Carlo simulation (*29*). The errors in the peak intensities for the simulation were determined from two independently measured relaxation data sets. NOE values were determined as the ratio of the steady-state intensities measured in the presence and absence of saturation of the proton magnetization, respectively.

For an initial estimate of the rotational correlation time (τ_m) and diffusion tensor (**D**), residues were selected on the basis of criteria outlined by Tjandra (*34*). Residues were rejected if the NOE was smaller than 0.60 or if the residues were potentially undergoing conformational exchange identified with the condition:

$$(\langle T_2\rangle - T_{2,n})/\langle T_2\rangle - (\langle T_1\rangle - T_{1,n})/\langle T_1\rangle > 1.5\sigma$$

where $T_{2,n}$ is the T_2 of residue n, $\langle T_2\rangle$ is the average T_2, and σ is the standard deviation of $(\langle T_2\rangle - T_{2,n})/\langle T_2\rangle - (\langle T_1\rangle - T_{1,n})/\langle T_1\rangle$. The measurements of cross-relaxation rates (η_{xy}) for excluding the residues undergoing conformational exchange (*35*) were not attempted because the statistical methods (*34*) are expected to give selection results similar to those of the experimental ones. The molecular rotational diffusion tensor (**D**) was estimated from the measured T_1/T_2 values and the solution structure of free wild-type KSI (*17*) or Y55F/Y88F complexed with 19-NTHS (*19*) as input structures. The calculations were performed by using the program R2R1_diffusion (*29*, *30*) for the cases of isotropic and axially symmetric diffusion tensors and the programs Quadratic_diffusion (*29*, *30*) and Tensor v. 1.1 (*36*) for the case of a fully anisotropic diffusion tensor.

The model-free parameters were selected by extensive Monte Carlo simulations and *F*-statistical testing, as described in the literature (*30*). The models and the optimized parameters were (1) S^2, (2) S_2 and τ_e, (3) S^2 and R_{ex}, (4) S^2, τ_e, and R_{ex}, and (5) S_s^2, S_f^2, and τ_s, where S^2 is the square of the generalized order parameter characterizing the amplitude of the internal motions, τ_e is the effective correlation time for the internal motions, R_{ex} is the exchange contribution to T_2, and the subscripts f and s indicate fast and slow time scales, respectively. The spectral density functions used for calculations of the relaxation data in an axially symmetric diffusion case are given by (*22*, *34*, *37*−*41*)

$$J(\omega) = \frac{2}{5}\left[S^2\sum_{j=1}^{3}\frac{A_j\tau_j}{1+(\omega\tau_j)^2}\right] \quad (1)$$

$$J(\omega) = \frac{2}{5}\left[S^2\sum_{j=1}^{3}\frac{A_j\tau_j}{1+(\omega\tau'_j)^2} + \frac{(1-S^2)\tau}{1+(\omega\tau)^2}\right] \quad (2)$$

$$J(\omega) = \frac{2}{5}\left[S^2\sum_{j=1}^{3}\frac{A_j\tau_j}{1+(\omega\tau_j)^2} + \frac{(S_f^2-S^2)\tau}{1+(\omega\tau)^2}\right] \quad (3)$$

where $\tau^{-1} = 6D + \tau_e^{-1}$, $\tau_1^{-1} = 6D_{\perp}$, $\tau_2^{-1} = 5D_{\perp} + D_{\parallel}$, $\tau_3^{-1} = 2D_{\perp} + 4D_{\parallel}$, $A_1 = (3\cos^2\theta - 1)^2/4$, $A_2 = 3\sin^2\theta\cos^2\theta$, $A_3 = (3/4)\sin^4\theta$, and θ is the angle between the N−H bond vector and the principal axis of the diffusion tensor. D is the isotropic diffusion constant, and $D_{\parallel}$ and $D_{\perp}$ are the components of the diffusion tensor parallel and perpendicular to the principal axis of the axial symmetry, respectively. The isotropic correlation time, τ_m, can be newly defined and is related to the isotropic diffusion constant D by $\tau_m = (6D)^{-1}$. The parameter A_j, which reflects the orientation of the amide N−H vector with respect to the principal axis of the diffusion tensor, was estimated from the solution structure of free wild-type KSI (*17*) or Y55F/Y88F complexed with 19-NTHS (*19*) as input structures. Equations 1, 2, and 3 were used for models 1, 2, and 5, respectively, and the additional R_{ex} term was introduced into eqs 1 and 2 for models 3 and 4. In model 5 (eq 3), $S^2 = S_s^2 S_f^2$, and the number of adjustable parameters is three for all five models. In the last stage of calculations, both the τ_m value and the $D_{\parallel}/D_{\perp}$ ratio were optimized simultaneously with all other model-free parameters.

RESULTS AND DISCUSSION

Comparison of ^{1}H and ^{15}N Chemical Shifts between Free and Complexed KSI. The assignments of backbone amide ^{1}H and ^{15}N chemical shifts of free KSI and its complex with 19-NTHS were initially carried out by comparing cross-peaks from heteronuclear single-quantum coherence (HSQC) spectra with the published assignments of free and 19-NTHS-bound Y55F/Y88F (*42*). The assignments were confirmed for most of the resolved peaks by the analysis of a 3D ^{15}N-edited NOESY and TOCSY. Ambiguous and too much overlapped peaks were eliminated during the assignment procedure.

Comparison of the chemical shifts between free and complexed KSI shows that there are large chemical shift changes both in the active site and in other regions upon ligand binding (Figure 2). One of the catalytic residues, Asp-38, shows the largest changes in both ^{1}H and ^{15}N chemical shifts. Large shift differences were also observed at the end of helix A3 (residues 48−61) and along β-strands B3 (residues 63−74), B4 (residues 77−88), B5 (residues 91−104), and B6 (residues 108−124). Such patterns in the shift differences are almost identical to the case of Y55F/Y88F (*42*). However, unlike the case of Y55F/Y88F, no changes were observed in the chemical shifts of the key catalytic residue, Tyr-14, upon ligand binding. According to the X-ray structure (*18*), Tyr-14, Tyr-55, bound-water molecules, and Asp-99 form a hydrogen-bonded network in free wild-type KSI. The negligible changes in the chemical shifts of Tyr-14 might be related to the hydrogen bond between Tyr-14 and Tyr-55, which could suppress structural changes of the amide group of Tyr-14 induced by the ligand binding.

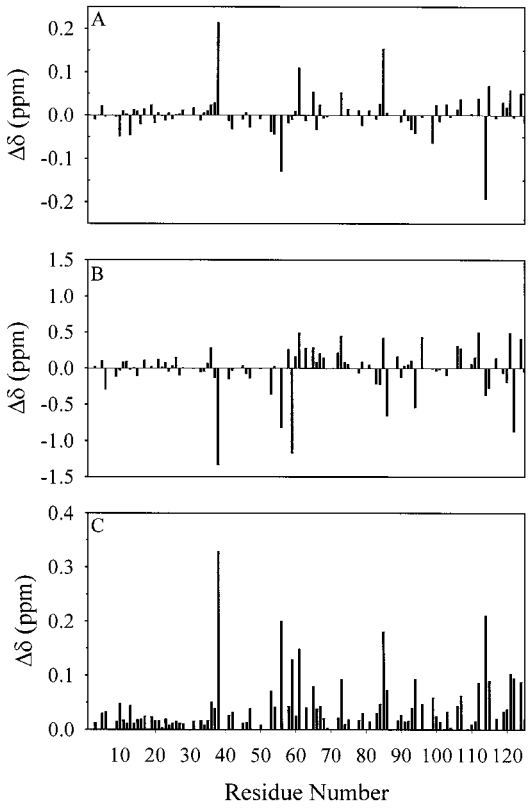

FIGURE 2: Backbone chemical shift differences between the free and 19-NTHS complexed KSI as functions of residue numbers. (A) Amide ^{1}H chemical shift differences. (B) Amide ^{15}N chemical shift differences. (C) Sum of the absolute magnitude of ^{1}H and ^{15}N chemical shift differences that were weighted according to the amide chemical shift dispersion in the ^{1}H and ^{15}N dimensions (3.11 and 27.3 ppm, respectively). The values for the free KSI are subtracted from those for the complexed KSI.

Molecular Rotational Diffusion Analysis of Free and Complexed KSI. To obtain the correct model-free parameters S^2, τ_e, and R_{ex}, it is necessary to estimate an exact value for the overall rotational correlation time, τ_m, from the ^{15}N T_1/T_2 ratio because small amounts of rotational anisotropy may contribute to R_{ex} (*34*). Ignoring rotational anisotropy can also lead to a distortion of the internal correlation time when the extended model-free formalism is required for an adequate fit (*32*, *43*). Therefore, an anisotropic model for rotational diffusion is essential in the case of highly asymmetric or multidomain proteins (*43*−*45*). Free KSI is highly asymmetric, having a relative ratio of 1.00:0.95:0.55 for the principal components of the inertia tensor based on the solution structure (*17*). The solution structure of Y55F/Y88F complexed with 19-NTHS (*19*) also gives a similar ratio of tensor values (1.00:0.93:0.56).

For an initial estimate of the rotational correlation time (τ_m) and diffusion tensor (**D**), residues were selected on the basis of criteria outlined by Tjandra (*34*). From a total of 91 and 90 residues whose relaxation parameters were measured, 67 and 60 residues were used to calculate the τ_m and diffusion parameters for free and complexed KSI, respectively. The statistical *F*-test indicates that the relaxation data are best described by an axially symmetric rotational diffusion tensor. Hence, the τ_m and $D_\parallel/D_\perp$ values from the axially symmetric model were used to analyze the internal motions of free KSI. After selection of appropriate internal dynamics models and final model-free calculations, the optimized effective τ_m was

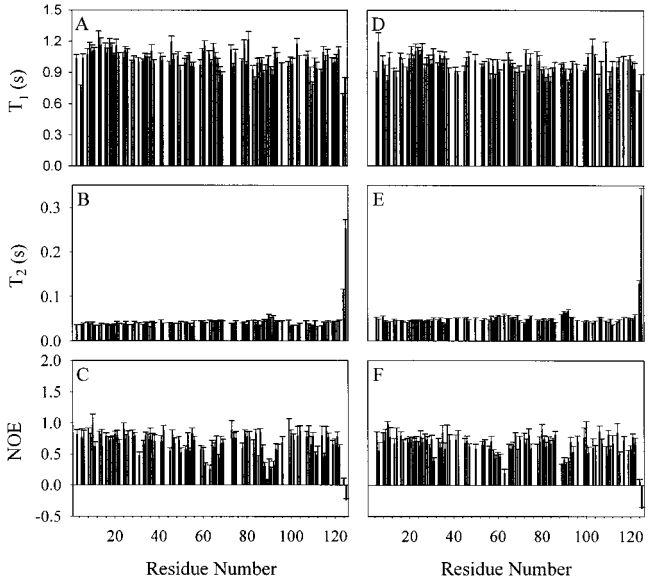

FIGURE 3: Plots of the measured ^{15}N relaxation parameters and their uncertainties as a function of residue number for the free (A−C) and 19-NTHS complexed KSI (D−F). (A, D) Longitudinal relaxation time T_1. (B, E) Transverse relaxation time T_2. (C, F) Heteronuclear NOE.

19.23 ± 0.08 ns with a diffusion anisotropy $D_\parallel/D_\perp = 1.26 \pm 0.03$. This value of τ_m is in good agreement with τ_m of 18.0 ns obtained by time-resolved fluorescence spectroscopic measurement for Y55F/Y88F (*46*) and the value of 20.1 ± 8.8 ns estimated by Stokes' law calculation.

The same calculation was performed on the complexed KSI, and the most acceptable model was also determined to be the axially symmetric one from *F*-test and Monte Carlo simulation. The calculated value of τ_m for the axially symmetric model from final optimization was 17.08 ± 0.07 ns with $D_\parallel/D_\perp = 1.25 \pm 0.03$. This value of τ_m for complexed KSI is somewhat smaller than that of free KSI, suggesting that KSI becomes more compact upon ligand binding. This result may corroborate the observations from the solution structure of Y55F/Y88F complexed with 19-NTHS that three α-helices become more closely packed onto the concave surface of the *β*-sheet upon ligand binding (*19*).

Backbone Dynamics of the Free KSI. Among the 120 residues in the KSI which can yield backbone amide signals (excluding the N-terminal methionine and the four prolines), 29 residues were excluded from the analysis due to resonance overlap or lack of signal intensity. Thus, quantitative ^{15}N relaxation measurements were carried out for 91 of the amide cross-peaks. The relaxation parameters T_1, T_2, and NOE for free KSI are shown in Figure 3A−C. For most residues, the T_1 and T_2 values lie in the ranges of 0.8−1.2 s and 35−55 ms, respectively. The heteronuclear NOEs for most of the residues were in the range of 0.6−0.9. In contrast, the two residues at the C-terminus show nearly zero or negative values. In addition, the NOEs for residues L61, L63, Y88, Q89, G90, R91, and K92, which are located between the secondary structure elements, were significantly smaller than the average, indicating that these linker regions are more mobile than the overall backbone.

The model-free analysis was performed with an axially symmetric rotational diffusion tensor. The model-free parameters S^2, τ_e, and R_{ex} for free KSI are shown in Figure

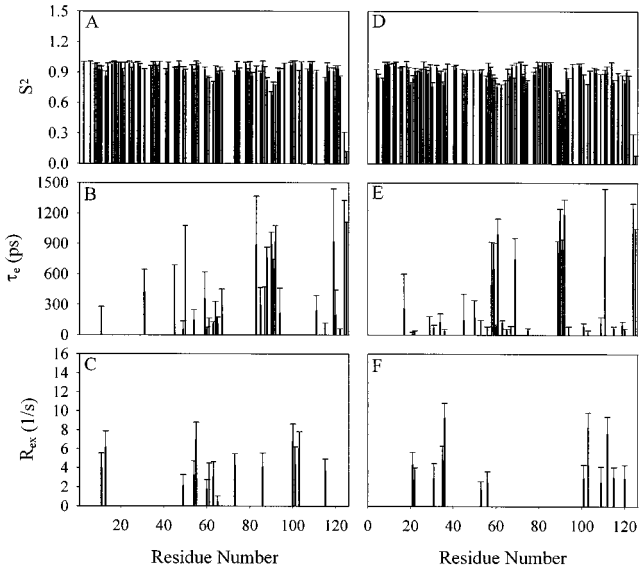

FIGURE 4: Plots of the model-free parameters and their uncertainties as a function of residue number for the free (A−C) and 19-NTHS-complexed KSI (D−F). (A, D) The generalized order parameter S^2. (B, E) The effective correlation time τ_e. (C, F) The chemical exchange contribution R_{ex}.

Table 1: Summary of Spectral Density Function Models Used To Fit T_1, T_2, and NOE Data for Free and Complexed KSI

model parameters	free	complexed
S^2	46	53
S^2 and τ_e	13	13
S^2 and R_{ex}	7	2
S^2, τ_e, and R_{ex}	8	11
S_s^2, S_f^2, and τ_s	7	10
not fit	10	1
total	91	90

4A−C. The spectral density models used to fit the relaxation data are summarized in Table 1. For most residues, the order parameters (S^2) are greater than 0.85, indicating that rapid motions on the fast (picosecond) time scale are highly restricted. The well-defined secondary structure elements, α-helices and β-strands, have average values for the order parameters of 0.95 ± 0.03 and 0.93 ± 0.03, respectively, which are slightly larger than the values found in most studies of protein dynamics using ^{15}N NMR relaxation measurements (*30*). In contrast, much lower order parameters were observed for the residues at the C-terminus (residues 124−125) and in the turn between strands B4 and B5 (residues 89−90).

The effective correlation times (τ_e) for internal motions were detected for 26 residues having values in the range of 50−1300 ps. Slower motions of τ_e on the time scale greater than 500 ps were found for residues 50, 88, 90, 91, 92, and 119 and the two C-terminal residues (124 and 125). Most of these residues are located in the turn or at the end of the secondary structure regions. The exchange term (R_{ex}), which reflects the existence of a dynamic exchange process in the microsecond to millisecond time scale (*47*), was detected for 15 residues, indicating that the motions on the micro- to millisecond time scale are relatively limited in free KSI.

Backbone Dynamics of the Complexed KSI. Relaxation measurements were carried out for 90 out of 120 backbone amide groups (excluding N-terminal methionine and 4 prolines) of the complexed KSI. The residual 30 residues were excluded from the analysis due to resonance overlap or lack of signal intensity. The relaxation parameters for complexed KSI are shown in Figure 3D−F. For most residues, the T_1, T_2, and NOE lie in the ranges of 0.8−1.2 s, 40−55 ms, and 0.6−0.9, respectively. The average T_1 in complexed KSI is slightly shorter than that in free KSI, while the T_2 is slightly longer. These data are consistent with the slightly smaller rotational correlation time for the complex compared to the free KSI.

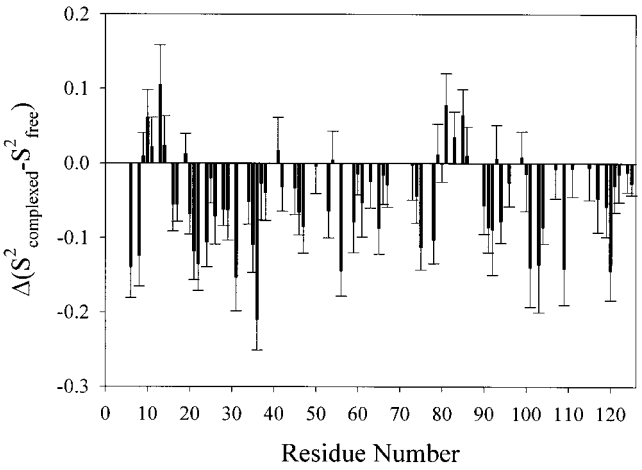

FIGURE 5: Differences between the generalized order parameters (S^2) for the free and 19-NTHS-complexed KSI. Only the residues whose relaxation parameters were determined in both free and complexed proteins were included in this plot.

The model-free parameters for complexed KSI are shown in Figure 4D−F. The average order parameters for the α-helices and β-strands are 0.91 ± 0.03 and 0.89 ± 0.04, respectively. These values are slightly smaller than those of free KSI, indicating that the complexed KSI has a relatively high degree of motion on the picosecond to nanosecond time scales compared to the free KSI. These observations are more consistent with those from the recent study of the C-terminal domain of *E. coli* DNA topoisomerase I (*16*), where reduced average order parameters for α-helices and β-sheets were observed upon ligand binding.

The effective correlation times (τ_e) were found for 34 residues in the range of 20−1300 ps. Slower motions of τ_e on the time scale greater than 500 ps were found for the residues at positions of 59, 61, 69, 89, 90, 91, 92, 111, 124, and 125. Most of these residues are again located in the turn or at the end of the secondary structure regions. Only 13 residues require the R_{ex} term for adequte fitting, which is similar to the case of free KSI. This result suggests that the motions on the micro- to millisecond time scale are relatively limited both in the free and in complexed KSI.

Comparison of the Backbone Dynamics in Free and Complexed KSI. The spectral density models used to fit the free and complexed KSI are summarized in Table 1. Relaxation data for most residues in free and complexed KSI are fit well using a simple model (S^2 only *or* S^2 and τ_e). Figure 5 shows the differences between the order parameters for the free and complexed KSI. The differences between the free and bound order parameters are larger than 0.05 in most residues, which are significant considering the average uncertainty of 0.024 in S^2. As shown in Figure 5, a number of residues have increased order parameters upon ligand binding, which are mainly located in helix A1 (residues

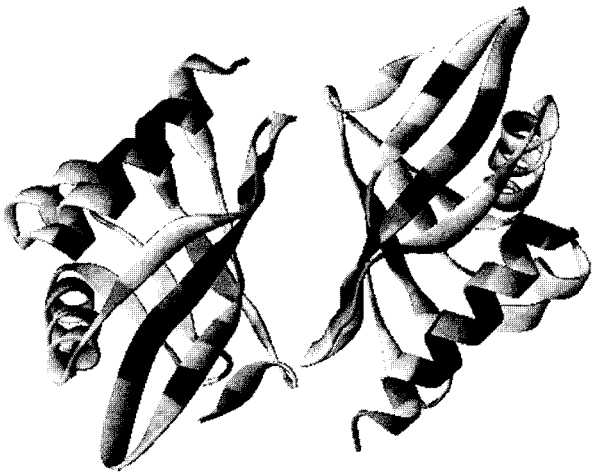

FIGURE 6: Ribbon diagram of KSI coded by the order parameter changes upon ligand binding. The residues for which S^2 increases are shown as black, the residues for which S^2 decreases are shown as white, and gray indicates those residues for which data for both free and complexed KSI are not available.

3−20) and strand B4 (residues 77−88), while the majority of the residues exhibit reduced order parameters, indicating the increased high-frequency (pico- to nanosecond) motions in the complexed KSI. Of course, it can be argued that the slight reduction of order parameter (and overall correlation time) is simply a result of the ligand binding breaking up a small degree of aggregation in the bound state. However, the enzyme sample did not show any sign of aggregation before and after the NMR experiments, and the diffusion anisotropies ($D_{\|}/D_{\perp}$), which might reflect the shape of protein, were almost the same (1.26 ± 0.03 and 1.25 ± 0.03) for the free and steroid-bound KSI. Furthermore, the aggregation and its breakup by the ligand binding would not explain the obvious increase in the order parameters for helix A1 and particularly strand B4. Thus, it would be reasonable to assume that the slight reduction of order parameter upon ligand binding is a genuine nature of KSI.

Figure 6 shows the ribbon diagram of the KSI backbone structure coded by the order parameter changes upon ligand binding in a gray scale manner. The residues for which S^2 increases upon ligand binding are shown as black, the residues for which S^2 decreases are shown as white, and gray indicates those residues for which data for both free and complexed KSI are not available. In the diagram, only those changes are considered significant which are larger than the average error of 0.024 in the order parameters. As can be seen in Figures 5 and 6, the effects of ligand binding on the dynamics of KSI are not local in nature but extend also to other regions. Thus, while the order parameters for helix A1 (residues 3−20) and strand B4 (residues 77−88) increase upon ligand binding, those of all other secondary structure elements decrease. The increase in the order parameters for helix A1 is not unexpected, since the key binding site residue, Tyr-14, is located at the center of this helix and the motions near the ligand binding site are typically restricted upon ligand binding. However, the increase in the order parameters for strand B4 is not expected considering that all other β-strands exhibit reduced order parameters. In addition, strands B3 (residues 63−74), B5 (residues 91−104), and B6 (residues 108−123), which have most of the 20 residues involved in the dimer interaction (*18*), exhibit reduced order parameters in the complexed KSI. These observations suggest that the 19-NTHS binding causes increased high-frequency (pico- to nanosecond) motions in the intersubunit region of this homodimeric enzyme. Similar results have been reported for 4-oxalocrotonate tautomerase (*10*), a 41 kDa homohexamer, for which the amide groups involved in *intersubunit* hydrogen bonds show increased mobility on ligand binding. Thus, the ligand binding loosened quaternary (intersubunit) interactions and tightened tertiary (intrasubunit) interactions. Our results are also more consistent with those from previous studies of the C-terminal SH2 domain of phospholipase C (*14*) or C-terminal domain of topoisomerase I (*16*), where decreased order parameters were observed upon binding to a phosphopeptide or single-stranded DNA, respectively. A decrease in order parameters for most residues in these proteins was attributed to the possibility that the ligand may exist in multiple conformations when bound.

In the active site, all three catalytic residues, Tyr-14, Asp-38, and Asp-99, exhibit high order parameters in complexed KSI, indicating severe restriction of the high-frequency internal motions. However, the dynamic behavior of Tyr-14, which is the direct binding site of 19-NTHS, is somewhat different from those of the other two catalytic residues, in which Tyr-14 exhibits a significant increase in the order parameter (0.956 vs 0.980) upon ligand binding, while those of Asp-38 and Asp-99 decreased (0.988 vs 0.949) or remained nearly constant (0.968 vs 0.976). This result suggests that Tyr-14 is involved more actively in the ligand binding than the other catalytic residues, which might have some implications on the enzyme mechanism. Nevertheless, since a study of the backbone dynamics gives only a partial picture of the changes that occur in the active site upon ligand binding, more studies including the side chain dynamics of all catalytic residues are needed.

CONCLUSIONS

We have investigated the complete backbone dynamics of free KSI and its complex with 19-NTHS by ^{1}H-detected ^{15}N relaxation rates and NOE determinations. Analysis of the relaxation data indicates that the high-frequency (pico- to nanosecond) motions are restricted upon 19-NTHS binding for a number of residues, which are mainly located in helix A1 and strand B4. However, the majority of the residues, especially those in strands B3, B5, and B6 involved in the dimer interaction, show reduced order parameters, indicating an increased mobility in the intersubunit region of this homodimeric enzyme. These results differ from the previous studies on the backbone dynamics of monomeric proteins, in which reduced mobilities are typically observed upon ligand binding, and may provide some insight into the dynamic behaviors of dimeric proteins.

SUPPORTING INFORMATION AVAILABLE

HN and ^{15}N chemical shifts, T_1, T_2, and steady-state ^{15}N-{^{1}H} NOEs for free (Table S1) and complexed (Table S2) KSI and model-free parameters for free (Table S3) and complexed KSI (Table S4) at 300 K. This material is available free of charge via the Internet at http://pubs.acs.org.

REFERENCES

1. Brutscher, B., Bruschweiler, B., and Ernst, R. R. (1997) *Biochemistry 36*, 13043−13053.

2. Farrow, N. A., Zhang, O., Forman-Kay, J. D., and Kay, L. E. (1997) *Biochemistry 36*, 2390−2402.
3. Mine, S., Tate, S., Ueda, T., Kainosho, M., and Imoto, T. (1999) *J. Mol. Biol. 286*, 1547−1565.
4. Lipari, G., and Szabo, A. (1982) *J. Am. Chem. Soc. 104*, 4546−4559.
5. Lipari, G., and Szabo, A. (1982) *J. Am. Chem. Soc. 104*, 4559−4570.
6. Kay, L. E., Muhandiram, D. R., Farrow, N. A., Aubin, Y., and Forman-Kay, J. D. (1996) *Biochemistry 35*, 361−368.
7. Yang, D., Mittermaier, A., Mok, Y.-K., and Kay, L. E. (1998) *J. Mol. Biol. 276*, 939−954.
8. Nicholson, L. K., Kay, L. E., Baldisseri, D. M., Arango, J., Young, P. E., Bax, A., and Torchia, D. A. (1992) *Biochemistry 31*, 5253−5263.
9. Zhao, Q., Abeygunawardana, C., and Mildvan, A. S. (1996) *Biochemistry 35*, 1525−1532.
10. Stivers, J. T., Abeygunawardana, C., Mildvan, A. S., and Whitman, C. P. (1996) *Biochemistry 35*, 16036−16047.
11. Hodsdon, M. E., and Cistola, D. P. (1997) *Biochemistry 36*, 2278−2290.
12. Olejniczak, E. T., Zhou, M. M., and Fesik, S. W. (1997) *Biochemistry 36*, 4118−4124.
13. Yuan, P., Marshall, V. P., Petzold, G. L., Poorman, R. A., and Stockman, B. J. (1999) *J. Biomol. NMR 15*, 55−64.
14. Farrow, N. A., Muhandiram, R., Singer, A. U., Pascal, S. M., Kay, C. M., Gish, G., Shoelson, S. E., Pawson, T., Forman-Kay, J. D., and Kay, L. E. (1994) *Biochemistry 33*, 5984−6003.
15. Zhang, W., Smithgall, T. E., and Gmeiner, W. H. (1998) *Biochemistry 37*, 7119−7126.
16. Yu, L., Zhu, C. X., Tse-Dinh, Y. C., and Fesik, S. W. (1996) *Biochemistry 35*, 9661−9666.
17. Wu, Z. R., Ebrahimian, S., Zawrotny, M. E., Thornburg, L. D., Perez-Alvarado, G. C., Brothers, P., Pollack, R. M., and Summers, M. F. (1997) *Science 276*, 415−418.
18. Cho, H. S., Choi, G., Choi, K. Y., and Oh, B.-H. (1998) *Biochemistry 37*, 8325−8330.
19. Massiah, M. A., Abeygunawardana, C., Gittis, A. G., and Mildvan, A. S. (1998) *Biochemistry 37*, 14701−14712.
20. Kim, S. W., Kim, C. Y., Benisek, W. F., and Choi, K. Y. (1994) *J. Bacteriol. 21*, 6672−6676.
21. Kuliopulos, A., Mildvan, A., S., Shortle, D., and Talalay, P. (1989) *Biochemistry 28*, 149−159.
22. Barbato, G., Ikura, M., Kay, L. E., Pastor, R. W., and Bax, A. (1992) *Biochemistry 31*, 5269−5278.
23. Grzesiek, S., and Bax, A. (1993) *J. Am. Chem. Soc. 115*, 12594−12595.
24. Piotto, M., Saudek, M., and Sklenar, V. (1992) *J. Biomol. NMR 2*, 661−665.
25. Wishart, D. S., Bigam, C. G., Yao, J., Abildgaard, F., Dyson, H. J., Oldfield, E., Markley, J. L., and Sykes, B. D. (1995) *J. Biomol. NMR 6*, 135−140.
26. Boyd, J., Hommel, U., and Campbell, I. D. (1992) *Chem. Phys. Lett. 175*, 477−482.
27. Kay, L. E., Keifer, P., and Saarinen, T. (1992) *J. Am. Chem. Soc. 114*, 10663−10665.
28. Palmer, A. G., III, Skelton, N. J., Chazin, W. J., Wright, P. E., and Rance, M. (1992) *Mol. Phys. 75*, 699−711.
29. Palmer, A. G., III, Rance, M., and Wright, P. E. (1991) *J. Am. Chem. Soc. 113*, 4371−4380.
30. Mandel, A. M., Akke, M., and Palmer, A. G., III (1995) *J. Mol. Biol. 246*, 144−163.
31. Rischel, C., Madsen, J. C., Anderson, K. V., and Poulsen, F. M. (1994) *Biochemistry 33*, 13997−14002.
32. Tjandra, N., Szabo, A., and Bax, A. (1996) *J. Am. Chem. Soc. 118*, 6986−6991.
33. Fushaman, D., and Cowburn, D. (1998) *J. Am. Chem. Soc. 120*, 7109−7110.
34. Tjandra, N., Feller, S. E., Paster, R. W., and Bax, A. (1995) *J. Am. Chem. Soc. 117*, 12562−12566.
35. Kroenke, C. D., Loria, J. P., Lee, L. K., Rance, M., and Palmer, A. G., III (1998) *J. Am. Chem. Soc. 120*, 7905−7915.
36. Dosset, P., Hus, J.-C., Blackledge, M., and Marion, D. (2000)- *J. Biomol. NMR 16*, 23−28.
37. Woessner, D. E. (1962) *J. Chem. Phys. 3*, 647−652.
38. Halle, B., and Wennerström, H. (1981) *J. Phys. Chem. 75*, 1928−1943.
39. Banci, L., Bertini, I., Cramaro, F., Conte, R. D., Rosato, A., and Viezzoli, M. S. (2000) *Biochemistry 39*, 9108−9118.
40. Zajicek, J., Chang, Y., and Castellino, F. J. (2000) *J. Mol. Biol. 301*, 333−347.
41. Sahu, S. C., Bhuyan, A. K., Majumdar, A., and Udgaonkar, J. B. (2000) *Proteins 41*, 460−474.
42. Zhao, Q., Abeygunawardana, C., and Mildvan, A. S. (1997) *Biochemistry 36*, 3458−3472.
43. Hansen, A. P., Petros, A. M., Meadows, R. P., and Fesik, S. W. (1994) *Biochemistry 33*, 15418−15424.
44. Bruschweiler, R., Liao, X., and Wright, P. E. (1995) *Science 268*, 886−889.
45. Mackay, J. P., Shaw, G. L., and King, G. F. (1996) *Biochemistry 35*, 4867−4877.
46. Wu, P., Li, Y. K., Talalay, P., and Brand, L. (1994) *Biochemistry 33*, 7415−7422.
47. Clore, G. M., Driscoll, P. C., Wingfield, P. T., and Gronenborn, A. M. (1990) *Biochemistry 29*, 7387−7401.

BI0023192